Published in final edited form as:
Cell Rep. 2013 August 29; 4(4): . doi:10.1016/j.celrep.2013.07.017.

Clathrin-Mediated Endocytosis Persists during Unperturbed Mitosis

Silvia K. Tacheva-Grigorova[1,7], **António J.M. Santos**[2,3,7], **Emmanuel Boucrot**[4,*], and **Tom Kirchhausen**[1,5,6,*]

[1]Program in Cellular and Molecular Medicine, Boston Children's Hospital, Boston, MA 02115, USA

[2]Section of Microbiology, MRC Centre for Molecular Bacteriology and Infection, Imperial College London, London SW7 2AZ, UK

[3]Graduate Program in Areas of Basic and Applied Biology (GABBA), University of Porto, Porto 4099-002, Portugal

[4]Institute of Structural and Molecular Biology, Division of Biosciences, University College London, London WC1E 6BT, UK

[5]Department of Cell Biology, Harvard Medical School, Boston, MA 02115, USA

[6]Department of Pediatrics, Harvard Medical School, Boston, MA 02115, USA

SUMMARY

How does mitosis influence the critical process of endocytosis? Some experiments lead to the conclusion that endocytosis arrests completely during mitosis, whereas others indicate that endocytosis persists. We have resolved this apparent discrepancy by showing how conditions of the experiment influence its outcome. The dynamics of clathrin-coated pit formation and the uptake of transferrin are maintained in naturally dividing cells but are nearly absent in mitotic cells arrested chemically by treatment with nocodazole, S-Trityl-L-cysteine, or RO-3306. Moreover, sequentially incubating cells at 4°C and then shifting them to 37°C or to serum starvation artificially increases the amount of transferrin receptor at the surface of naturally dividing cells, leading to the incorrect conclusion that endocytosis has ceased during mitosis. Thus, our data show that endocytosis is unaffected during all stages of natural cell division.

INTRODUCTION

The elaborate regulation of molecular events during cell division extends to membrane organization and membrane traffic. The changes in shape that accompany the generation of two cells from one obviously require extensive redirection of membrane components. Control of endocytosis and exocytosis (i.e., the uptake and redeposition of membrane components at the cell surface) must underlie these processes. The exit from metaphase

*Correspondence: e.boucrot@ucl.ac.uk(E.B.), kirchhausen@crystal.harvard.edu(T.K.).
[7]These authors contributed equally to this work

SUPPLEMENTAL INFORMATION

Supplemental Information includes one figure and can be found with this article online at http://dx.doi.org/10.1016/j.celrep.2013.07.017.

appears to be a critical control point, just as it is for spindle activity and chromosome separation.

Long-standing dogma holds that membrane traffic stalls during mitosis. Support for this view derives primarily from two sets of observations: (1) transient dissolution of the Golgi apparatus during cell division, and (2) decreased endosomal recycling and inhibition of clathrin-mediated transferrin uptake and fluid-phase uptake, particularly during metaphase. One paper provided morphological evidence for stalled endocytosis by showing the absence of detectable coated pits in mitotic A431 cells (Pypaert et al., 1987). Cell physiological evidence supporting this conclusion came from imaging-based experiments that compared the amount of fluorescent ligand or fluid-phase marker captured by mitotic and by interphase cells and showed that a substantially decreased amount was internalized by mitotic cells that were undergoing natural cell division or were chemically arrested with nocodazole (Berlin and Oliver, 1980; Berlin et al., 1978; Oliver et al., 1985; Quintart et al., 1979; Raucher and Sheetz, 1999; Sager et al., 1984). One short-coming of these studies was their failure to normalize the uptake by the amount of available surface membrane. This issue is particularly relevant because there is a substantial decrease in surface membrane when cells round up and prepare to divide. We previously showed that modulation of endosomal recycling during cell division controls the cell area and downregulates the surface expression of some membrane-bound proteins (Boucrot and Kirchhausen, 2007). We found that whereas clathrin-mediated endocytosis was normal throughout all phases of cell division, recycling of internalized membrane decreased sharply during metaphase and reactivated in anaphase. We proposed that this simple mechanism accounted for the large reduction in surface area that accompanied the transformation of a relatively extended interphase cell to a rounded mitotic cell. We found that uptake of a fluid phase marker (dextran), corrected by the amount of available surface area, was similar in mitotic and interphase cells. We also found that transient endosomal retention of internalized transferrin receptor (TfR) during metaphase led to its disappearance from the cell surface, thereby explaining the apparent reduction of transferrin uptake. The experiments from which these conclusions derived involved direct analysis of single HeLa and BSC1 cells undergoing natural cell division over a period of ~1 hr. We used live-cell fluorescence imaging to follow the dynamics of fluorescently tagged AP2 adaptors marking endocytic clathrin-coated pits. We also determined the endocytic uptake and surface expression of TfR and other ligands by fluorescence microscopy in cells maintained at 37°C throughout the experiment. Confirmation of these dynamics for clathrin-coated pits and vesicles during mitosis came from subsequent work from another laboratory on mouse keratinocytes undergoing natural cell division (Devenport et al., 2011).

In a recent study, Fielding et al. (2012) reached the opposite view, proposing that clathrin-mediated endocytosis stops during mitosis. Using a combination of flow cytometry and fluorescence microscopy of fixed samples, the authors found strongly inhibited uptake and concomitant surface accumulation of two sets of endocytic probes: TfR and CD8-chimeras containing the ectodomain and transmembrane segment of CD8 fused to a cytosolic segment containing endocytic-sorting motifs recognized by the clathrin machinery. In their study, they used cells that were undergoing natural mitosis, were chemically arrested in mitosis by addition of nocodazole, which depolymerizes spindle microtubules (Zieve et al., 1980), or were synchronized by washout of the CDK1 inhibitor RO-3306, which arrests cells at the G2/M transition (Vassilev et al., 2006).

To understand the experimental circumstances that could explain the different conclusions drawn from these two sets of results, we tested whether differences between protocols could influence endocytosis. We confirmed that endocytosis is unaltered during metaphase in HeLa and BSC1 cells undergoing natural mitosis. We found that the compounds used to

generate mitotic arrest or mitotic synchrony strongly affected the clathrin pathway. Mitotic arrest produced by treatment with nocodazole (as described by Fielding et al., 2012) or S-Trityl-L-cysteine (STLC, an Eg5 kinase inhibitor; Skoufias et al., 2006) eliminated coated pits at the plasma membrane. RO-3306 washout, also as described by Fielding et al. (2012), led to increased coated pit lifetimes during mitosis in the synchronized cells. We further found that the temperature shift in a one-cycle endocytic assay, in which cells were incubated with ligand at 4°C and then warmed to 37°C to allow endocytosis to proceed, produced a substantial increase in surface TfR, which was particularly noticeable in naturally dividing mitotic cells. Because the endocytic rate is calculated as the ratio between internalized ligand and its receptor at the cell surface, increased surface expression following a temperature shift yields an erroneous decrease in the calculated endocytic rate.

RESULTS

Coat Dynamics Are Unaffected during Natural Mitosis

All endocytic plasma membrane coated pits and vesicles appear to contain the clathrin adaptor AP2 in mammalian cells expressing normal levels of coat proteins imaged under conditions of steady-state, clathrin-mediated endocytosis (Boucrot et al., 2010; Ehrlich et al., 2004). We previously showed that the dynamics of AP2 incorporation into plasma membrane clathrin-coated pits and vesicles is the same during natural cell division and interphase (Boucrot and Kirchhausen, 2007). As before, in this work we used live-cell, spinning-disc confocal fluorescence microscopy imaging with high temporal resolution to image HeLa and BSC1 cells as they transitioned from inter-phase to metaphase and then to cytokinesis. AP2 in these cells was fluorescently tagged by stable expression of σ2-EGFP, its small adaptin subunit (Ehrlich et al., 2004). In Figure 1A, representative images from rapidly acquired (~1.5 s) three-dimensional (3D) stacks spanning the full height of metaphase cells show the free top surface, the free middle equatorial region, and the surface attached to the coverslip. In all cases we found AP2 fluorescent spots, characteristic of endocytic clathrin-coated structures, over the entire cell surface. As we showed previously (Boucrot and Kirchhausen, 2007), the membrane density of AP2 spots (equivalent to clathrin-coated structures) remained constant during interphase, metaphase, and cytokinesis (Figure 1B). We also found a reduction in the number of AP2 spots on the cell membrane of metaphase cells (Figure 1C), reflecting the transient decrease in total plasma membrane area during this stage of the cell cycle (Boucrot and Kirchhausen, 2007). To illustrate that the coat dynamics is the same during different stages, we performed an extensive analysis using data derived from 2 min, 3D time series of AP2 from the top and bottom surfaces of HeLa and BSC1 dividing cells (Figures 1D–1F). The kymographs in Figure 1D illustrate characteristic AP2 traces corresponding to rapidly forming canonical coated pits (examples highlighted by orange arrowheads) on the top and bottom surfaces of cells imaged during both interphase and metaphase. The kymographs also show the presence of longer-lived coated plaques at the bottom surface, particularly in HeLa cells (white arrowheads in Figure 1D; quantification in Figure 1E, upper portion; Saffarian et al., 2009). As before, we found that the canonical coats were equally dynamic, irrespective of the stage of cell division (interphase, metaphase, and cytokinesis). The coats had similar lifetimes (the time from initiation to coated-vesicle budding; Figure 1E) and similar maximum fluorescence intensities immediately before coat disassembly occurred (an indication of coated-vesicle size (Figure 1F; Ehrlich et al., 2004; Saffarian et al., 2009), Thus, the time needed to form a coated pit and for it to bud as a coated vesicle is uniform throughout the cycle of a naturally dividing cell.

Absence of Coat Dynamics in Chemically Arrested Mitotic Cells

Some of the endocytosis experiments reported by Fielding et al. (2012) involved either mitotic arrest by treating the cells with nocodazole or enrichment of cells in metaphase by washing out previously added RO-3306. Using data primarily from flow cytometry of mitotic cells arrested by a 16 hr exposure to nocodazole or during the washout period (30 min) after an 18 hr incubation with RO-3306, they found that receptor-mediated uptake of fluorescent transferrin or various chimeric CD8 endocytic probes (monitored with a CD8 fluorescently tagged antibody) was blocked in mitotic cells. Based on the significant increase of TfR and the chimeric probes at the cell surface, they concluded that the failure to internalize was due to inhibition of the clathrin endocytic machinery.

We show here that the clathrin-based endocytic machinery indeed is strongly impaired in chemically arrested mitotic HeLa and BSC1 cells. Using spinning-disc confocal live-cell imaging to follow the dynamics of endocytic coat formation in cells treated with nocodazole, we detected no fluorescent AP2 spots at the surface of cells arrested in mitosis. Representative optical slices acquired using the fast 3D imaging protocol from the bottom and top surfaces and the equatorial middle section of natural and chemically arrested mitotic HeLa and BSC1 cells are shown in Figure 2A, and quantitation of these data is shown in Figure 2B. The absence of endocytic coated pits in the mitotic cells could not be accounted for by a direct effect of nocodazole on coat assembly, because AP2 spots were clearly detected in interphase cells and their lifetime was the same in interphase cells whether or not they had been treated with nocodazole (Figure 2D). The loss of AP2 at the membrane in mitotic-arrested cells was accompanied by the expected increase in diffuse cytosolic signal (bottom, Figures 2A and 2C). Treatment of HeLa and BSC1 cells with STLC, another compound used to arrest cells in metaphase (Skoufias et al., 2006), also resulted in full loss of membrane-associated AP2 spots in the mitotic cells (Figures 2A–2D). As with nocodazole treatment, the presence of STLC had no detectable influence on the lifetime of endocytic clathrin/AP2 coats in interphase cells and minimally increased the number of stalled pits at the top surface of mitotic HeLa cells (Figure 2D).

We also followed the protocol used by Fielding et al. (2012) to generate mitotic cells that appeared during washout of RO-3386, which arrests cells at the G2/M transition. In contrast to the mitotic cells arrested by treatment with nocodazole or STLC, these metaphase cells contained dynamic AP2 spots, but the lifetimes of these spots were somewhat longer than those in untreated control cells and similar to those in cells that remained in interphase during the RO-3386 treatment (Figures 2C and 2D). In contrast to nocodazole or STLC, washout of RO-3386 significantly increased the number of stalled pits in mitotic and interphase HeLa and BSC1 cells during the washout period (Figure 2D), as well as during constant incubation (not shown).

These experiments show that the mitotic arrest induced by treatment with nocodazole or STLC strongly impairs the formation of endocytic coated pits and coated vesicles, thus explaining why Fielding et al. found that such cells fail to internalize transferrin or the chimeric CD8 endocytic probe in cells chemically arrested in mitosis. The increased time required to form a coated vesicle, combined with the increased stalling of endocytic coated pits in cells treated with RO-3386, also explains the decreased clathrin-mediated cargo uptake described by Fielding et al.

Surface Expression of TfR Decreases in Cells Undergoing Natural Mitosis, but Not in Chemically Arrested Mitotic Cells

We previously showed a substantial decrease in the surface expression of TfR in BSC1 cells undergoing natural metaphase, an observation that we interpreted to be consistent with

normal maintenance of clathrin-mediated endocytosis and inhibition of endosomal recycling (Boucrot and Kirchhausen, 2007). Here, we extended that analysis and examined the surface expression of transferrin in HeLa, BSC1, HEK293, and RPE1 cells undergoing normal mitosis (Figures 3A and S1), and compared HeLa cells undergoing normal mitosis with those arrested in metaphase by treatment with RO-3306, nocodazole, or STLC (Figure 3C). We used laser scanning confocal microscopy to determine the amount of available receptors at the surface by visualizing the binding of a fluorescently labeled antibody specific for the ectodomain of TfR. The cell-division stage was determined by the shape of the cells and by the appearance of the chromatin as visualized with the DNA dye DRAQ5. We acquired optical sections at the bottom surface and the middle equatorial section, and compared the fluorescence signal of the bound TfR antibody in metaphase cells with the signal in interphase cells (present in the same visualization field) acquired using the same imaging parameters. We quantified these experiments by integrating the surface signal from optical sections covering the entire cell (Figures 3B and 3D).

We first confirmed our earlier observations and showed that in all cases there was substantially less TfR at the cell surface of metaphase cells compared with interphase cells (Figure 3A, orange arrowhead and quantification in Figure 3B; see also Figures 3C and 3D, “asynchronous”). We then investigated the effects of nocodazole, STLC, and RO-3306 on TfR surface expression. In agreement with Fielding et al. (2012), we found the same amount of TfR on the surface of the mitotic HeLa cells exposed to the inhibitors as on interphase cells (Figures 3C and 3D). In contrast, the control for these experiments, which we carried out using naturally occurring mitotic cells, showed a pronounced decrease in TfR surface expression (Figures 3C and 3D, “asynchronous”).

We then determined the efficiency of receptor-mediated internalization of transferrin by measuring the endocytic rate of transferrin (Figure 4), defined by the amount of fluorescent transferrin internalized during a given period normalized by the level of TfR at the cell surface (Ghosh et al., 1994; Spiro et al., 1996; Wiley and Cunningham, 1982). As shown in Figure 4A, the endocytic rate followed the expected asymptotic behavior in both interphase and naturally dividing cells. We confirmed our earlier observations showing similar endocytic rates for interphase and metaphase BSC1 cells (Boucrot and Kirchhausen, 2007), and found the same result for HeLa cells (Figures 4B and 4C). However, mitotic HeLa cells that were chemically arrested by treatment with RO-3306, nocodazole, or STLC were greatly impaired in transferrin uptake. Transferrin uptake by interphase cells was not affected by RO-3386 or nocodazole, but we noted a small reduction in cells treated with STLC, in accord with the dynamics of coated pit formation determined in similarly treated BSC1 cells (Figure 2D). These results agree with our earlier finding that transferrin is internalized with similar efficiencies in interphase and naturally dividing cells, and also with the observations of Fielding et al. (2012) showing that uptake is halted in mitotic cells synchronized by chemical treatment.

A Temperature Shift from 4°C to 37°C or Incubation with Serum-Free Medium Artificially Increases the Amount of TfR at the Cell Surface

The transient decrease in the amount of TfR at the surface of mitotic cells undergoing asynchronous natural division is clearly in conflict with the similar surface levels of TfR (and also of a CD8-based recombinant chimeric receptor) during all stages of cell division reported by Fielding et al. (2012). A key difference between our internalization protocol and theirs is that we did not employ a shift in temperature during the experiment. The assay we use (Spiro et al., 1996) is based on a protocol that was first described by Wiley and Cunningham (1982), in which the cells are kept at 37°C during all steps of the endocytic assay, including the brief period (minutes) of incubation with the ligand. We determine the amount of surface receptor at the end of the experiment by incubating the cells at 4°C with

the ligand or with antibody specific for the ectodomain of the receptor. The one-cycle endocytic assay used by Fielding et al. requires prebinding of the ligand to cells for ~30 min at 4°C, followed by brief warming (minutes) to 37°C, during which time endocytosis ensues. We show here that rewarming leads to a substantial increase in cell-surface TfR, particularly in mitotic cells (Figures 5A and 5B, 30′ at 4°C). We also found a similar increase in cell-surface TfR in cells that were incubated for 45 min with serum-free medium lacking transferrin and were maintained at 37°C (Figures 5A and 5B, 45′serum free), as well as when serum starvation preceded a 4°C to 37°C shift (Figure 5B, 45′ serum free + 30′ at 4°C). The latter protocol was included in the experiments carried out by Fielding et al. (2012).

The unexpected increase in the amount of TfR at the surface of cells exposed to the temperature shift or serum starvation resulted in a substantial lowering of the calculated endocytic rate for interphase and an even more accentuated decrease in metaphase cells (Figure 5C). Thus, the one-cycle endocytic rate measurement should be avoided because it can yield an erroneously low value, particularly in mitotic cells.

DISCUSSION

We show here that there are important differences in the dynamics of the endocytic clathrin machinery and in TfR internalization, and between cells undergoing natural mitosis and cells arrested in mitosis by treatment with nocodazole or STLC or observed in mitosis after synchronization by washout of RO-3306. Endocytic coated pits and vesicles are absent in mitotic cells arrested with nocodazole or STLC, and are retarded in mitotic cells synchronized with RO-3306, but the dynamics of coated pits and vesicles is normal in naturally dividing cells. We also show an increase in surface TfR (and perhaps of other recycling receptors) after a temperature shift from 4°C to 37°C. This upregulation of surface TfR, after the ligand-binding step required for a one-cycle internalization assay, is particularly noticeable in mitotic cells and leads to an incorrectly low estimate of the endocytic rate.

We reproduced the flow-cytometry observations of Fielding et al. (2012), who reported that transferrin uptake was blocked in chemically arrested mitotic cells despite an approximately normal level of TfR at the cell surface. The surface accumulation of TfR in nocodazole- and STLC-mitotic arrested cells and the blocked transferrin uptake are consistent with the absence of coated pits detectable by live-cell imaging. The surface accumulation and inhibition of transferrin uptake in mitotic cells immediately after removal of RO-3306 are likewise consistent with the significantly longer lifetimes of coated pits and with the increased number of stalled coated pits in those cells. The inhibitory effects of nocodazole and STLC were restricted to cells in metaphase, as we saw no such inhibition in interphase cells similarly exposed to these compounds. One possible explanation for the failure to form coated pits in cells locked for a long time in mitosis is a large increase in membrane tension resulting from continuous removal of the membrane at the cell surface accompanied by inhibition of endosomal membrane recycling. RO-3306 interfered with coat formation even in cells that remained in interphase. Further analysis will reveal whether or not their increased lifetime is a direct effect of Cdk1 inhibition.

Using four different cell types, we have shown that the decrease in transferrin uptake observed during metaphase is due to the substantial reduction in the amount of TfR available at the surface of cells undergoing natural mitosis (Boucrot and Kirchhausen, 2007; Warren et al., 1984). This decrease results from transient capture of the receptor in endosomal structures due to inhibition of the recycling pathway from endosomes back to the cell surface (Boucrot and Kirchhausen, 2007; Warren et al., 1984). These results are at odds with

the data of Fielding et al. (2012), who clearly found high levels of TfR or chimeric CD8 endocytic probes at the cell surface of naturally dividing cells. As we have shown here, however, there are two experimental conditions that can induce an abrupt increase in the levels of TfR at the cell surface: (1) a shift from 4°C to 37°C following the ligand-binding step at 4°C, as used in the one-cycle internalization assay, and (2) a 45 min incubation of cells with serum-free medium, which is often used to clear bound ligand prior to commencement of an endocytic assay. The upregulation of TfR is particularly noticeable in naturally dividing cells, which display low levels of TfR at the cell surface when they are not perturbed by a temperature shift or serum starvation. The upregulation presumably results from uncontrolled fusion at the cell surface of endosomes retained in the cell during metaphase (Boucrot and Kirchhausen, 2007). We do not yet have an explanation for these observations, and we also do not know whether other membrane receptors are similarly upregulated. Nonetheless, one should avoid conditions that lead to such experimentally induced upregulation, particularly when attempting to determine endocytic rates, as the rate calculation involves correction of the amount of internalized ligand by the amount of receptor at the cell surface. Using the receptor level obtained under conditions of acute upregulation will erroneously provide a low endocytic rate, particularly when the extent of endocytosis is rate limiting, as is the case for mammalian cells in tissue culture conditions in which only 1%–3% of the surface receptors are internalized every minute (Hansen et al., 1992).

Another important issue that is not ordinarily considered in estimations of the relative internalization efficiency of fluid-phase markers or ligands of cells in metaphase and other stages during the cell cycle is the reduction in surface area due to rounding observed in mitotic cells. This reduction can be substantial (6 × in BSC1 cells and 2 × in HeLa cells; Boucrot and Kirchhausen, 2007). Not considering the surface-area reduction can easily explain the apparent “decrease” of internalized ligand or fluid-phase markers observed during mitosis. To our knowledge, such a correction is absent in the published literature (Berlin and Oliver, 1980; Berlin et al., 1978; Oliver et al., 1985; Quintart et al., 1979; Raucher and Sheetz, 1999; Sager et al., 1984; Fielding et al., 2012). When the correction is applied to the uptake of dextran by mitotic cells, it shows that the internalization of this fluid-phase marker is maintained during all stages of cell division (Boucrot and Kirchhausen, 2007). It also shows that the surface density of assembling coated pits is about the same in metaphase and interphase cells (Boucrot and Kirchhausen, 2007; this study).

In conclusion, based on our current findings, we suggest that studies of membrane traffic, particularly during cell division, are best carried out under normal conditions and that investigators should avoid the use of long-term exposure of compounds such as nocodazole, STLC, and RO-3306, or cells that have been exposed to drastic temperature shifts or serum starvation.

EXPERIMENTAL PROCEDURES

Cell Culture and Asynchronous and Chemical Synchronization of Cell Division

Human HeLa, monkey BSC1, and human HEK293 cells were grown at 37°C and 5% CO_2 in Dulbecco’s modified Eagle’s medium (DMEM; GIBCO) containing L-glutamine and 10% fetal calf serum (FCS). Normal diploid human RPE1 cells (ATCC CRL-4000) were grown at 37°C and 5% CO_2 in DMEM:F12 HAM (Sigma) supplemented with 0.25% (w/v) sodium bicarbonate (Sigma), 1 mM glutamine (Sigma), and 10% FCS. HeLa and BSC1 cells stably expressing σ2-EGFP (the small subunit of AP2 fused to EGFP) were described earlier (Ehrlich et al., 2004). Enrichment in the number of cells undergoing natural mitosis (used for live-cell imaging experiments) was achieved ~17 hr after replating of HeLa or BSC1 cells that were previously arrested in their growth by contact inhibition (Boucrot and

Kirchhausen, 2007). For fixed-cell experiments (transferrin uptake and receptor surface levels), no enrichment of cells undergoing natural mitosis was performed. Cells were chemically synchronized in mitosis by treatment with 40 ng/ml nocodazole (Sigma) for 16 hr or with 9 μM RO-3306 for 18 hr followed by a 30 min release in normal medium (Fielding et al., 2012). Cells were also synchronized in mitosis by incubation with 9 μMSTLC for 18 hr (Skoufias et al., 2006). Different stages of cell division were established by morphology for live-cell imaging experiments and complemented by DNA visualization with 5 μM DRAQ5 (Biostatus) for fixed samples.

Antibodies

The primary antibody used was rabbit anti-TfR (CBL47; Chemicon). Alexa488-or Alexa555-conjugated antibodies were used as secondary antibodies (Invitrogen).

Transferrin Uptake and TfR Cell-Surface Staining

In most cases, cells grown on #1.5 glass coverslips were continuously incubated at 37°C with 50 μg/ml Alexa488 transferrin (Invitrogen) in prewarmed imaging medium (α-MEM, 5% fetal bovine serum, 20 mM HEPES pH 7.4) for the indicated time (7–30 min). In some cases, cells were first incubated with 50 μg/ml Alexa488 transferrin in serum-free α-MEM at 4°C (on ice) for 30 min before they were transferred to 37°C. In other cases, cells were incubated in serum-free medium for 45 min prior to the endocytic assays described above. At the end of the 37°C incubation period used to follow endocytosis, the cells were cooled to 4°C, washed twice with ice-cold PBS to remove unbound transferrin, and then incubated twice for 2 min at 4°C with ice-cold stripping buffer (150 mM NaCl, 20 mM HEPES, 5 mM KCl, 1 mM $CaCl_2$, 1 mM $MgCl_2$, pH 5.5) to remove transferrin bound to the cell surface. The cells were then washed once with ice-cold PBS and then incubated for 1 hr at 4°C with a solution containing rabbit TfR antibody (diluted 1:500 from the stock) in α-MEM (to stain the receptor at the cell surface). The samples were washed in ice-cold PBS and then fixed at 4°C with ice-cold 3.7% paraformal-dehyde in PBS for 20 min, followed with three washes with PBS and one wash with PBS supplemented with 50 mM NH_4Cl. Finally, the cells were incubated for 1 hr at 20°C with PBS containing anti-rabbit secondary antibody and 5 μM DRAQ5. In some experiments, fixed cells were only labeled with the TfR antibody without permeabilization and stained with an anti-rabbit secondary Alexa488 antibody (surface staining). Total fluorescence in both channels (corresponding to the amount of TfR at the cell surface and the amount of internalized Tf) was determined by integrating the fluorescence originating from the cell surface membrane and the cell interior on all planes of the 3D stack corrected for background.

Live-Cell Spinning-Disc Confocal Fluorescence Microscopy

Cells stably expressing σ2-EGFP were plated on 25-mm-diameter glass #1.5 coverslips and imaged using phenol red-free α-MEM medium supplemented with 10% FCS and 20 mM HEPES pH 7.4. The coverslips were placed in a humidified chamber (20/20 Technologies) at 37°C, equilibrated with 5% CO2, and imaged using a Mariana system (Intelligent Imaging Innovations, 3I) based on an Axiovert 200M inverted microscope (Carl Zeiss) with a 63 × objective lens (Plan-Apochromat, NA 1.4; Carl Zeiss) and a CSU-22 spinning-disc confocal unit (Yokogawa Electric) upgraded with a Borealis system equipped and illuminated with a 50 mw, 491 nm solid-state laser. The illumination power leaving the objective was adjusted to 2.9 mw. The images were acquired with a CCD camera (QuantEM: 512SC; Photometrics) without binning and a final optical magnification of 94.5 ×. The imaging system and acquisition of two-dimensional (2D) and 3D time series were controlled with the use of Slidebook 5 (3i).

The live-cell imaging protocol consisted of the following steps: (1) A cell undergoing metaphase was identified by bright-field illumination. (2) A spinning-disc confocal 3D stack composed of a sufficient number of consecutive optical sections spaced 0.5 μmapart to fully include the complete height of the cell (each frame acquired with 30 ms exposures) was acquired. (3) A 3D time series comprised of a z stack of six consecutive optical sections spaced 0.5 μm from the bottom (attached) surface, followed by a similar four-dimensional (4D) time series from the free (dorsal) surface, was acquired. Each series was acquired for 120 s at a frequency of 0.3 Hz and with 30 ms exposures; a 2D time series was then generated from the maximum-intensity z projection obtained for each time point. (4) Steps 2 and 3 were repeated following cytokinesis and prior to abscission. (5) Cells undergoing interphase were imaged separately from metaphase cells. In this case, we acquired two 120-s-long time series: first a 2D time series comprised of a single optical section corresponding to the bottom surface (30 ms exposure), and then a 4D time series corresponding to the top surface of the same cell followed by generation of a 2D time series made of the maximum-intensity z projection obtained for each time point. Fluorescence AP2 spots were identified and tracked with the use of IMAB (Massol et al., 2006).

Fixed-Cell Laser Scanning Confocal Microscopy

Fixed samples were imaged with a laser scanning confocal microscope (TCS Sp5 AOBS; Leica) equipped with a 63 × objective. For Alexa488, the illumination was at 488 nm and emission was collected between 498 and 548 nm. For Alexa555, the laser illumination was at 543 nm and emission was collected between 555 and 620 nm. For Alexa647 and DRAQ5, the laser illumination was at 633 nm and emission was collected between 660 and 746 nm. Each channel was acquired sequentially. 3D stacks comprising the whole volume of the cell were acquired using optical sections spaced 0.5 μm apart. All experiments were performed, acquired, and analyzed similarly.

Statistical Tests

The statistical significance for differences between the data was established using a two-tailed Student’s t test. Data are expressed as the average ± SD.

Supplementary Material

Refer to Web version on PubMed Central for supplementary material.

Acknowledgments

We thank E. Marino for maintaining the imaging resources in the Kirchhausen laboratory and R. Massol for making IMAB available. This work was supported in part by NIH grants GM-075252 (to T.K.) and U54 AI057159 (New England Regional Center of Excellence in Biodefense and Emerging Infectious Disease, Core Imaging Facility), the Fundação para a Ciência e Tecnologia (to A.J.M.S.), and a Biological Sciences Research Council (BBSRC) David Phillips Research Fellowship (to E.B.).

REFERENCES

Berlin RD, Oliver JM. Surface functions during mitosis. II. Quantitation of pinocytosis and kinetic characterization of the mitotic cycle with a new fluorescence technique. J. Cell Biol. 1980; 85:660–671. [PubMed: 6156175]

Berlin RD, Oliver JM, Walter RJ. Surface functions during Mitosis I: phagocytosis, pinocytosis and mobility of surface-bound Con A. Cell. 1978; 15:327–341. [PubMed: 719746]

Boucrot E, Kirchhausen T. Endosomal recycling controls plasma membrane area during mitosis. Proc. Natl. Acad. Sci. USA. 2007; 104:7939–7944. [PubMed: 17483462]

Boucrot E, Saffarian S, Zhang R, Kirchhausen T. Roles of AP-2 in clathrin-mediated endocytosis. PLoS ONE. 2010; 5:e10597. [PubMed: 20485680]

Devenport D, Oristian D, Heller E, Fuchs E. Mitotic internalization of planar cell polarity proteins preserves tissue polarity. Nat. Cell Biol. 2011; 13:893–902. [PubMed: 21743464]

Ehrlich M, Boll W, Van Oijen A, Hariharan R, Chandran K, Nibert ML, Kirchhausen T. Endocytosis by random initiation and stabilization of clathrin-coated pits. Cell. 2004; 118:591–605. [PubMed: 15339664]

Fielding AB, Willox AK, Okeke E, Royle SJ. Clathrin-mediated endocytosis is inhibited during mitosis. Proc. Natl. Acad. Sci. USA. 2012; 109:6572–6577. [PubMed: 22493256]

Ghosh RN, Gelman DL, Maxfield FR. Quantification of low density lipoprotein and transferrin endocytic sorting HEp2 cells using confocal microscopy. J. Cell Sci. 1994; 107:2177–2189. [PubMed: 7983176]

Hansen SH, Sandvig K, van Deurs B. Internalization efficiency of the transferrin receptor. Exp. Cell Res. 1992; 199:19–28. [PubMed: 1735458]

Massol RH, Boll W, Griffin AM, Kirchhausen T. A burst of auxilin recruitment determines the onset of clathrin-coated vesicle uncoating. Proc. Natl. Acad. Sci. USA. 2006; 103:10265–10270. [PubMed: 16798879]

Oliver JM, Seagrave JC, Pfeiffer JR, Feibig ML, Deanin GG. Surface functions during mitosis in rat basophilic leukemia cells. J. Cell Biol. 1985; 101:2156–2166. [PubMed: 2933415]

Pypaert M, Lucocq JM, Warren G. Coated pits in interphase and mitotic A431 cells. Eur. J. Cell Biol. 1987; 45:23–29. [PubMed: 2894988]

Quintart J, Leroy-Houyet MA, Trouet A, Baudhuin P. Endocytosis and chloroquine accumulation during the cell cycle of hepatoma cells in culture. J. Cell Biol. 1979; 82:644–653. [PubMed: 511930]

Raucher D, Sheetz MP. Membrane expansion increases endocytosis rate during mitosis. J. Cell Biol. 1999; 144:497–506. [PubMed: 9971744]

Saffarian S, Cocucci E, Kirchhausen T. Distinct dynamics of endocytic clathrin-coated pits and coated plaques. PLoS Biol. 2009; 7:e1000191. [PubMed: 19809571]

Sager PR, Brown PA, Berlin RD. Analysis of transferrin recycling in mitotic and interphase HeLa cells by quantitative fluorescence microscopy. Cell. 1984; 39:275–282. [PubMed: 6498936]

Skoufias DA, DeBonis S, Saoudi Y, Lebeau L, Crevel I, Cross R, Wade RH, Hackney D, Kozielski F. S-trityl-L-cysteine is a reversible, tight binding inhibitor of the human kinesin Eg5 that specifically blocks mitotic progression. J. Biol. Chem. 2006; 281:17559–17569. [PubMed: 16507573]

Spiro DJ, Boll W, Kirchhausen T, Wessling-Resnick M. Wortmannin alters the transferrin receptor endocytic pathway in vivo and in vitro. Mol. Biol. Cell. 1996; 7:355–367. [PubMed: 8868465]

Vassilev LT, Tovar C, Chen S, Knezevic D, Zhao X, Sun H, Heimbrook DC, Chen L. Selective small-molecule inhibitor reveals critical mitotic functions of human CDK1. Proc. Natl. Acad. Sci. USA. 2006; 103:10660–10665. [PubMed: 16818887]

Warren G, Davoust J, Cockcroft A. Recycling of transferrin receptors in A431 cells is inhibited during mitosis. EMBO J. 1984; 3:2217–2225. [PubMed: 6209129]

Wiley HS, Cunningham DD. The endocytotic rate constant. A cellular parameter for quantitating receptor-mediated endocytosis. J. Biol. Chem. 1982; 257:4222–4229. [PubMed: 6279628]

Zieve GW, Turnbull D, Mullins JM, McIntosh JR. Production of large numbers of mitotic mammalian cells by use of the reversible micro-tubule inhibitor nocodazole. Nocodazole accumulated mitotic cells. Exp. Cell Res. 1980; 126:397–405. [PubMed: 6153987]

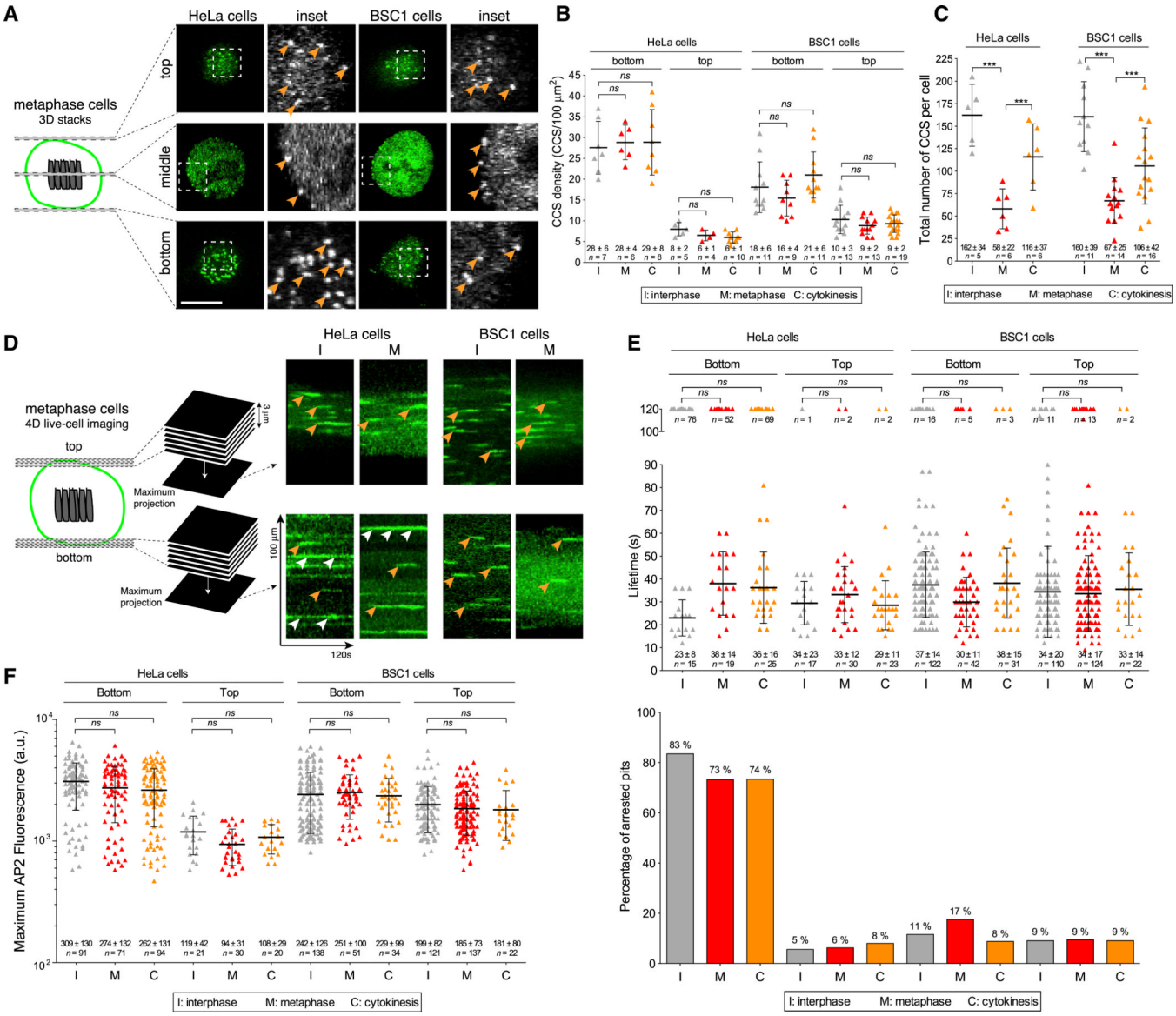

Figure 1. Coat Dynamics Are Not Affected during Natural Mitosis

(A) Schematic representation of the 3D visualization strategy used to image metaphase cells, and visualization examples showing AP2 spots corresponding to endocytic clathrin/AP2-coated pits and vesicles (arrowheads); z stacks were obtained by imaging sequential planes spaced 0.5 µm apart. The examples correspond to images obtained by spinning-disc confocal fluorescence microscopy from the top and bottom surfaces and the middle equatorial planes of metaphase HeLa and BSC1 cells stably expressing σ2-EGFP. The scale bar represents 10 µm.

(B) Surface density of clathrin/AP2-coated structures (CCS/100 µm^2) calculated from the number of AP2 spots at the top and bottom surfaces of HeLa and BSC1 cells imaged during interphase, metaphase, and cytokinesis prior to abscission. Bars and numerical values are averages ± SD; n, number of cells; ns, no statistical difference ($p > 0.05$).

(C) Total number of clathrin/AP2-coated structures (CCS per cell) on the plasma membrane of a cell as determined by counting the number of fluorescent AP2 spots detected in each

whole z stack obtained by 3D live-cell imaging. Bars and numerical values are averages ± SD; n, number of cells; ***$p < 0.0001$.

(D) Schematic representation of the 4D visualization strategy. The examples are kymograph representations obtained from 2D time series corresponding to maximum-intensity z-projection sets from 4D time series acquired using spinning-disc confocal microscopy. The examples illustrate the temporal behavior of AP2 spots at the top and bottom surfaces of HeLa and BSC1 cells stably expressing σ2-EGFP. Orange and white arrowheads highlight canonical coated pits and plaques, respectively.

(E) Upper panel: plot of the individual lifetimes of clathrin/AP2 pits from HeLa and BSC1 cells calculated from 4D time series obtained from the bottom and top surfaces during metaphase and cytokinesis, or from 2D and 4D time series from the bottom and top surfaces of interphase cells. At least five cells were imaged for each condition. Bars and numerical values are averages ± SD; n, number of AP2 spots. Lower panel: fraction of AP2 spots (percentage of arrested pits) whose lifetime was longer than the time series (120 s) corresponding to the data in the upper panel.

(F) Plot of individual maximum fluorescence signals of AP2 spots obtained from the time series used to calculate the data in (E).

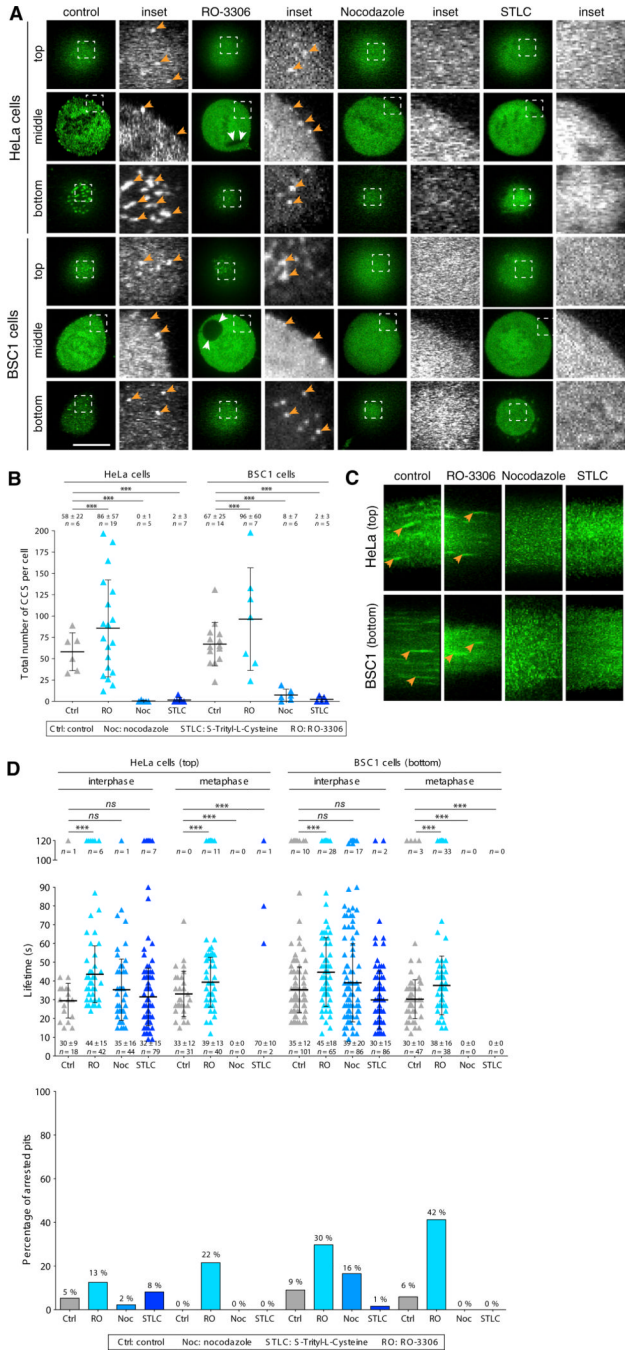

Figure 2. Absence of Coat Dynamics in Chemically Arrested Mitotic Cells

(A) Images obtained by spinning-disc confocal fluorescence microscopy from the top and bottom surfaces and middle equatorial planes of HeLa and BSC1 cells stably expressing σ2-EGFP undergoing natural mitosis (control), during the washout period after treatment with RO-3306, or after chemical arrest during mitosis by nocodazole or STLC treatment. Examples of AP2 spots (orange arrowheads) are shown. Note the complete absence of clathrin/AP2-coated pits and vesicles in mitotic cells arrested by nocodazole or STLC. RO-3306 treatment results in the formation of large intracellular vacuoles (white arrowheads). The scale bar represents 10 μm.

(B) Total number of clathrin/AP2 structures (CCS per cell) on the plasma membrane of the cell as determined by counting the number of fluorescent AP2 spots detected in the complete z stack of each cell obtained by 3D live-cell imaging. Averages ± SD; n, number of cells; ***$p < 0.0001$.

(C) Representative kymographs showing clathrin/AP2 dynamics from 4D time series obtained by live-cell spinning disc confocal acquired from the top of HeLa or bottom surfaces of BSC1 cells stably expressing σ2-EGFP during natural mitosis (control), mitotic cells imaged during the washout period after treatment with RO-3306, or mitotic cells arrested by incubation with nocodazole or STLC. Examples of AP2 tracks are highlighted (arrowhead).

(D) Upper panel: plot of the individual lifetimes of clathrin/AP2 pits from HeLa and BSC1 cells calculated from 4D time series obtained from the bottom and top surface of metaphase or from 2D and 4D time series from the top and bottom surfaces of interphase cells. At least five cells were imaged for each condition. Bars and numerical values are averages ± SD; n, number of AP2 spots. Lower panel: fraction of AP2 spots whose lifetime was longer than the time series (120 s) used to calculate the data in the upper panel (percentage of arrested pits). ***$p < 0.0001$; ns, not significant ($p > 0.05$).

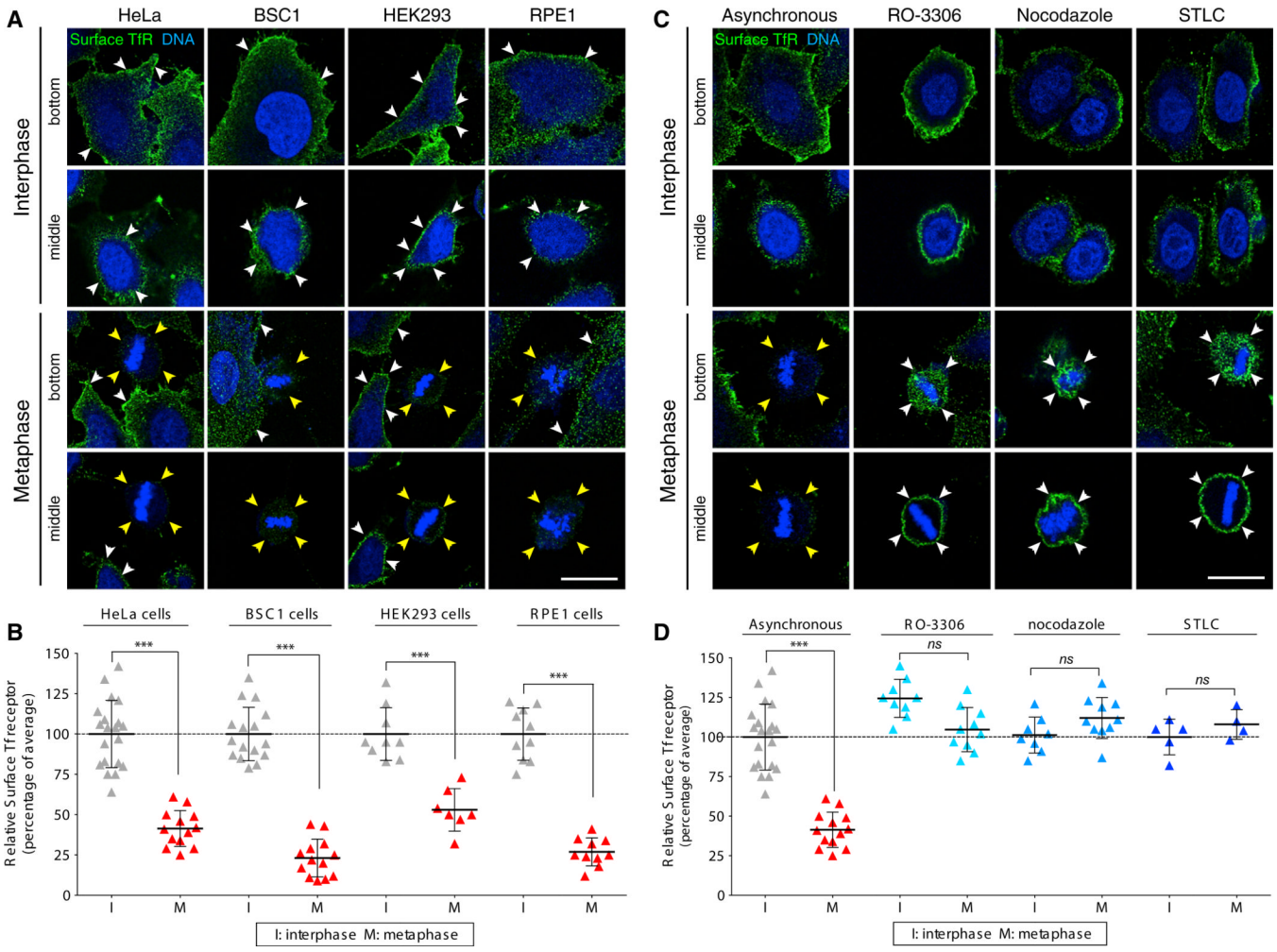

Figure 3. The Surface Expression of TfR Decreases Transiently in Cells Undergoing Natural Mitosis, but Not in Cells Arrested in Metaphase by Chemical Synchronization

(A) Representative images of HeLa, BSC1, HEK293, and RPE1 cells during interphase and metaphase undergoing natural mitosis, obtained by laser-scanning confocal microscopy. The views are from the bottom surface and the middle equatorial section of the same cell surface labeled with an antibody specific for the ectodomain of the TfR (green) and stained for DNA (blue). Note the significantly lower intensity of the fluorescence signal of TfR at the surface of naturally dividing metaphase cells (yellow arrowheads) compared with interphase cells (white arrowheads). The scale bar represents 10 μm.

(B) Plot of the relative fluorescence signal of the antibody specific for the ectodomain of TfR determined during different stages of natural division of individual cells visualized as described in (A). Data for each cell type were normalized to the average intensity during interphase and correspond to a total of 55 and 43 cells in interphase and metaphase, respectively.

(C) Data obtained by laser-scanning confocal microscopy of HeLa cells during interphase, during natural mitosis (asynchronous), synchronized in mitosis during the washout of RO-3306, and arrested in mitosis by treatment with nocodazole or STLC. Representative views show the surface content of TfR at the bottom surface and middle equatorial section of the same cell imaged using an antibody specific for the ectodomain of the TfR (surface TfR, green) and DNA (blue). Note the significantly lower fluorescence signal of TfR at the surface of naturally dividing metaphase cells (yellow arrowheads) compared with the higher

signal in chemically treated metaphase cells (white arrowheads). The scale bar represents 10 μm.

(D) Plot of the relative fluorescence signal of the antibody specific for the ectodomain of TfR in individual cells visualized as described in (A). Data for each condition were normalized to the average of the intensities of the control cells during interphase; 42 and 37 cells in interphase and metaphase, respectively, were analyzed. Bars are averages ± SD. ***$p < 0.0001$; ns, not significant ($p > 0.05$). See also Figure S1.

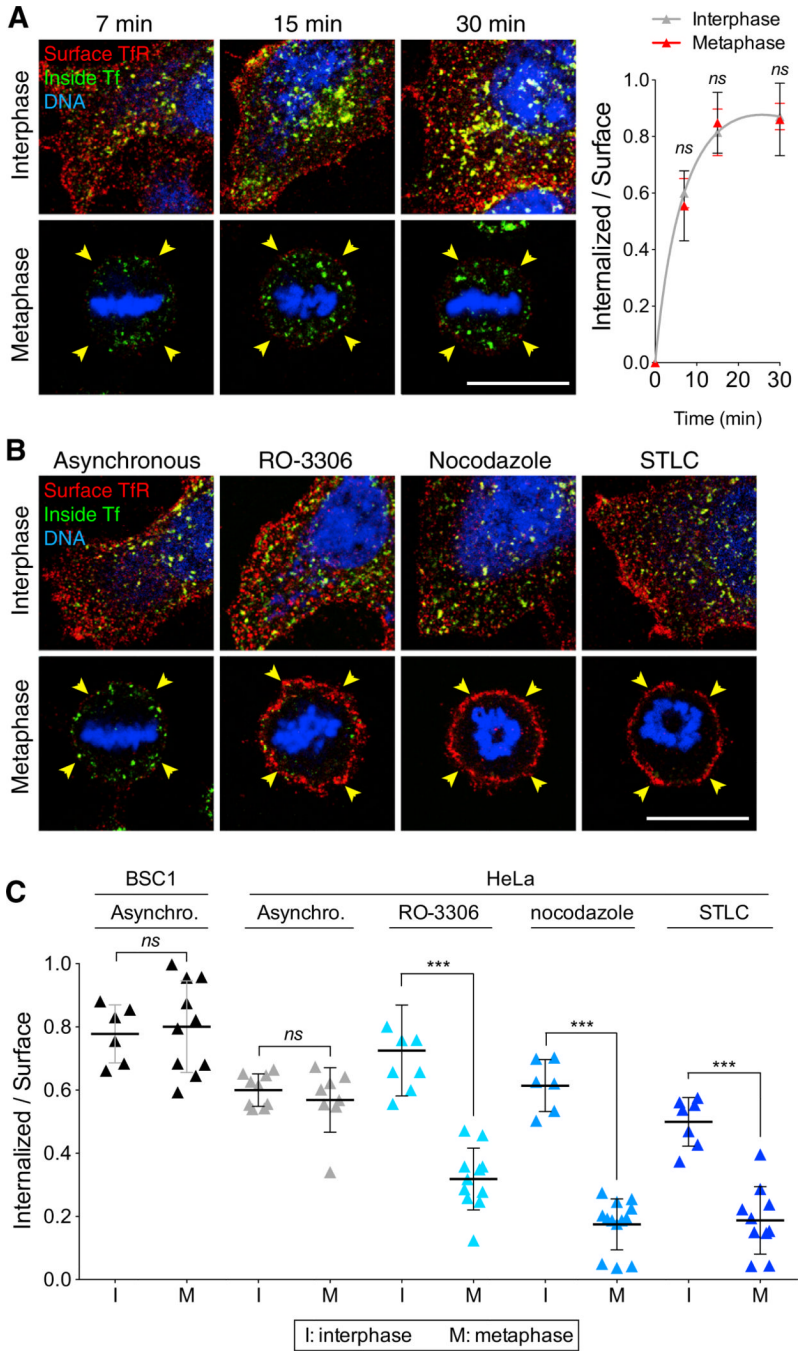

Figure 4. Effect of Chemical Synchronization on the Endocytic Rate of the TfR of Mitotic Cells

(A) Representative middle equatorial images of internalized Tf and TfR at the surface of BSC1 cells during interphase or undergoing natural mitosis after incubation for the indicated times with transferrin-Alexa488 (inside Tf; green) and subsequent antibody staining of TfR (surface TfR, red) and DNA (blue). Bar: 10 μm. The corresponding plot shows the ratio between the fluorescence signals of Tf and TfR at the cell surface calculated at the indicated times of continuous endocytosis. The amount of internalized Tf corresponds to the total value integrated throughout the whole volume of 40 and 36 cells in interphase (gray) and naturally dividing mitotic cells (red), respectively. The initial slope of the curves

corresponds to the endocytic rate; data points are averages ± SD. ns, not significant ($p > 0.05$).

(B) Representative middle-equatorial section images of internalized Tf and TfR at the cell surface in the absence or presence of RO-3306, nocodazole, or STLC. The images were obtained after incubation for 7 min with transferrin-Alexa488 (inside Tf, green) and subsequent staining for surface TfR (surface TfR, red) and DNA (blue). Note the accumulation of internalized Tf and low surface TfR in the asynchronous metaphase cell, and the absence of internalized Tf and high surface TfR in all chemically arrested mitotic cells. Scale bar, 10 μm.

(C) Plot of endocytic rates obtained from the experiment described in (B). Bars are averages ± SD. ns, not significant ($p > 0.05$). ***$p < 0.0001$.

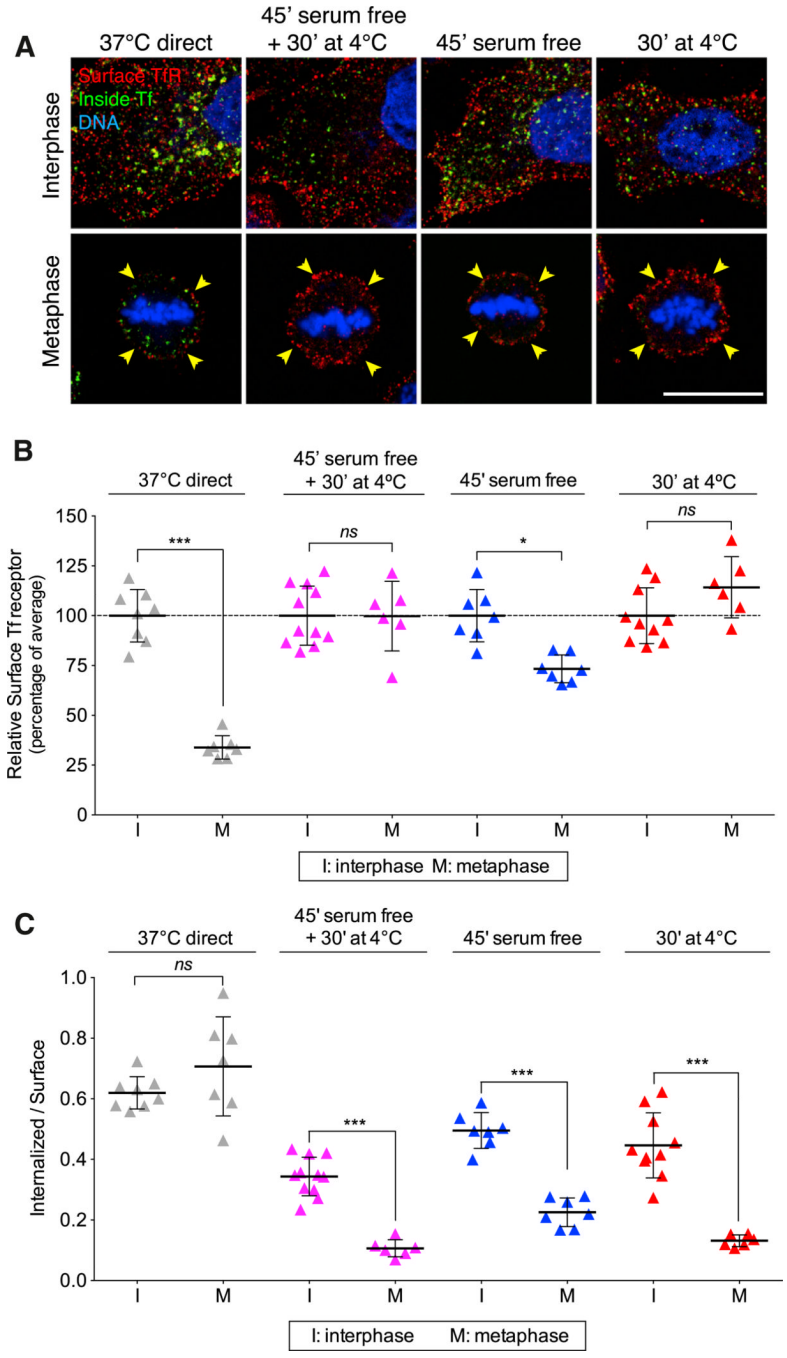

Figure 5. Increase in the Level of Surface TfR of Mitotic Cells Induced by a 4°C to 37°C Temperature Shift or by Incubation with Serum-Free Medium

(A) Representative middle-equatorial sections of BSC1 cells showing transferrin- Alexa488 (inside Tf; green) internalized after 7 min incubation at 37°C and subsequently stained with an antibody for cell-surface TfR (surface TfR; red) at 4°C for 30 min. Prior to these steps, cells were kept at 37°C (37°C direct) or incubated in serum-free medium for 45 min at 4°C (45′ serum free + 30′ at 4°C), in serum free-medium for 45 min at 37°C (45′ serum free), or with medium containing serum at 4°C for 30 min (30′at 4°C). Cells were also stained for DNA (blue). Note the significant increase of surface TfR in mitotic cells subjected to temperature shift or serum-free conditions. The scale bar represents 10 μm.

(B) Plot of fluorescence signal corresponding to surface TfR for the experiment described in (A). Data for each condition were normalized to the average intensity of control interphase cells; 36 and 26 cells in interphase and metaphase, respectively, were analyzed.
(C) Plot of endocytic rates obtained from the experiment described in (B). The values were obtained by integration of the fluorescence signals corresponding to internalized Tf and surface TfR throughout the whole cell volume; 36 and 26 cells in interphase and metaphase, respectively, were analyzed. Bars are averages ± SD. ns, not significant ($p > 0.05$); *$p < 0.01$; ***$p < 0.0001$.